International Journal of Fluid Power 11 (2010) No. 1 pp. 7-19

EXPERIMENTAL MODELLING AND CONTROL OF A SERVO-HYDRAULIC FORCE CONTROL SYSTEM

Joseph Kennedy and Roger Fales

Rolf Fluid Power Lab
University of Missouri-Columbia, Department of Mechanical and Aerospace Engineering, Columbia, Missouri 65211
jlkz67@mizzou.edu, FalesR@missouri.edu

Abstract

The objective of this work is to model a hydraulic force control servo system and then improve upon the performance of the system through feedback control design. The hydraulic system is first constructed and tested. Experimental data based linear models of the system are found through input-output measurements. The models contain a right-half-plane zero; therefore, a bandwidth limitation is placed on the control design (i.e., the bandwidth frequency of the control system is limited). Three types of controllers (*P*, *PID* and H_∞) are designed specifically for the linear models. The closed-loop time domain and frequency domain performance of each control system is found and compared for the models and system. Uncertainties and performance weights are finally used in finding the nominal/robust stability and performance.

Keywords: force control, robustness, performance, servo

1 Introduction

Servo-valves are used within hydraulic control systems to accurately regulate the output of the entire system. The valve provides the interface between the hydraulic power unit and the output device, in this case a linear actuator. The control valve has the ability to receive a signal from a control system in order for the output of the system to track a desired input (Manring, 2005). Using force feedback to control a hydraulic system allows the user to control the force output from a linear actuator by supplying the control system with a desired force reference signal. Controllers are designed specifically for the closed-loop (CL) system to improve performance and robustness.

There are many types of controllers that can be implemented into a CL control system, each of which adds different performance characteristics. The process used in this paper for obtaining CL control is as follows. Linear models representing the open-loop (OL) frequency domain performance of the servo system are found through analyzing input-output measurements at given operating points over a range of frequencies. Controllers are designed specifically for the linear models and then tested on the servo system to find the CL time and frequency domain performance of the system. Once a control system is designed and tested, the nominal/robust stability and performance of that control system can be found. The nominal stability and performance are found in relation to the nominal plant (i.e., the linear model). The uncertainties within the OL system (both dynamic and parametric) are used in finding a perturbed plant. This perturbed plant along with a performance weight transfer function (TF) is used in evaluating the robust stability and performance.

Hydraulic actuators have several non-linearities due mainly to servo-valve flow and pressure characteristics (Niksefat and Sepehri, 1999). The method used in this work is based on the linearization of the non-linear dynamics of a hydraulic system about given operating points. The stability and performance of a linear control system is, therefore, only achievable at or near the operating points which the controller is designed around. In order to model a full range of operating points, a different method must be considered. One such method considers non-linear Quantitative Feedback Theory (QFT) where the non-linear plant is replaced with a "family of linear time invariant transfer functions" (Niksefat and Sepehri, 1999). The linear TF's are based on experimental input-output measurements similar to the procedure taken in this work. Non-linear QFT robust control methodology is then used to

This manuscript was received on 18 June 2009 and was accepted after revision for publication on 18 January 2010

design a force controller that is of "low-order" and that can "maintain satisfactory performance against uncertainties" (Niksefat and Sepehri, 1999). A second method for modelling an entire system uses Input-Output Feedback Linearization, which requires full state feedback (Chiriboga et al., 1995). In this approach, no specific operating point is used in obtaining a linear model. Therefore, the performance of a given control system is not influenced by its proximity to the set of operating points, which results in better performance over the entire operating range of the system (Chiriboga et al., 1995). Either method discussed here can be implemented if the linear method does not result in satisfactory performance due to the uncertainties of the system and/or if a wide range of operating points are needed.

The movement of the main loading actuator is restricted in this work (i.e., the load dynamics are very stiff). Applications for this type of configuration include testing platforms for material compression/tensile strength and small strain fatigue cycle testing. For these testing rigs, a combination of good performance and robustness is desired to reduce the respective cycle times and percent overshoot (large overshoots can cause the ultimate stress of the material to be exceeded). Dynamic testing units with force ranges near ± 5500 lbf [± 24,465 N] have bandwidth frequencies from 15 to 55 Hz with 80 % load (MTS Systems, 2009 and Instron, 1998). Similarly, the system discussed in this work provides approximately ± 5000 lbf [± 22,241 N]. Therefore, the control systems designed in this work will attempt to fall within bandwidth range given above.

Alternatively, the experimental setups given by Niksefat and Sephehri (1999), Rito (2006), and Alleyne (1999) allow actuator movement through the use of springs or secondary actuators (i.e., the load dynamics of these systems are significantly smaller than when actuator movement is restricted). Alleyne (1999) also describes the performance limitations of force control due to the existence of left-half-plane (LHP) zeros. In contrast, the existence of right-half-plane (RHP) zeros and their influence on system performance is discussed in this work. The experimental setup in this work also incorporates a needle valve to regulate hydraulic fluid flow between the high and low-pressure side of the actuator (Niksefat and Sephehri (1999), Rito (2006), nor Alleyne (1999) provide such a feature). Finally, this work gives extensive uncertainty analysis on the control systems that the references mentioned above do not.

2 Experimental Setup

A picture and schematic of the hydraulic servo system are shown in Fig. 1 and 2, respectively. A double-rod actuator is used as the force output device. The rear, *B*, actuator rod is enclosed within a protective casing. The front, *A*, actuator rod is connected to a load cell, which in turn is attached to a stiff steel link. The link is bolted to a bracket that is secured to the same I-beam as the actuator, impeding actuator movement during loading. There is a slight actuator movement (2.8 x 10^{-5} m max) due mainly to the stiffness of the connecting rod (this movement is neglected in the analytical analysis of the system). Two pressure sensors are placed on either side of the piston to record fluid pressures within the actuator (i.e., P_A and P_B in Fig. 2). A third pressure sensor records the supply pressure, P_{su}, from the hydraulic power unit. The power unit uses an electric motor and hydraulic pump to supply the system with a constant P_{su}. A hydraulic line connects side *A* and *B* of the actuator allowing hydraulic fluid to leak from the high to low-pressure side. A needle valve is placed on the leakage line to control the amount of fluid that can be passed from one side of the actuator to the other.

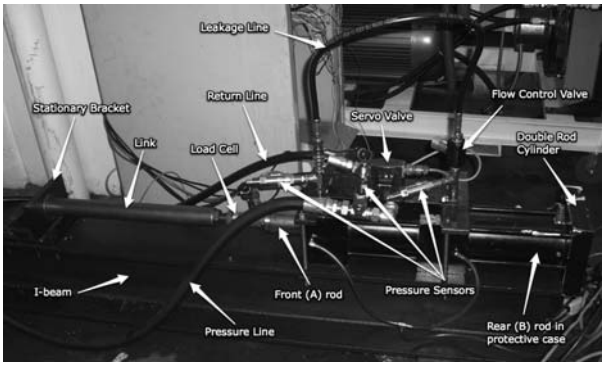

Fig. 1: *Hydraulic servo system*

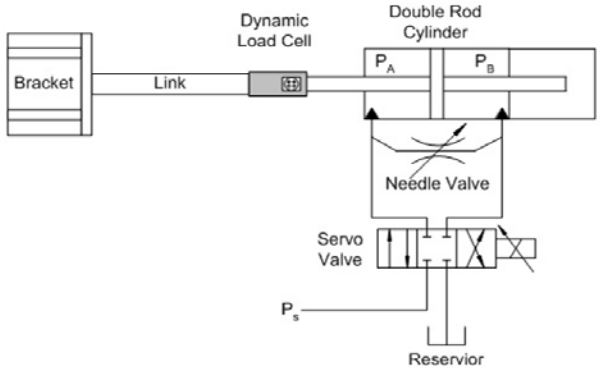

Fig. 2: *Schematic of the servo system*

The servo-valve is a MTS model #252.25A with a flow rate of 15 gpm [9.46 x 10^{-4} m^3/sec] at 1000 psi [6.895 MPa] and a nominal bandwidth of 170 Hz. An input voltage to the servo-valve amplifier causes a displacement of the electric actuator, which results in a movement of the internal spool. As the spool displacement increases, a larger differential pressure is created within the actuator, resulting in a larger force output. The needle valve behaves as an orifice; therefore, the cross-sectional area within the valve, A_o, has a direct correlation to the volumetric flow rate given as

$$Q = A_o C_d \sqrt{\frac{2}{\rho}\Delta p} \tag{1}$$

where C_d is the discharge coefficient, ρ is the fluid density and Δp is the pressure difference across the orifice. Increasing A_o increases the flow through the

needle valve. For the output force to remain constant, the servo-valve drive must supply (or make up for) this flow.

The hydraulic power unit supplies the servo system with a constant P_{su} of 1000 psi [6.895 MPa]. The double-rod actuator has a piston area of 5.23 in^2 [9.46 x 10^{-3} m^2]. Therefore, the max/min output force from the actuator is approximately ± 5200 lbf [± 23,131 N]. With no leakage through the needle valve (there still exists cross-piston leakage due to the servo-valve itself), the system has a high gain over all frequencies (i.e., a small voltage results in a large force output). This causes a large sensitivity in the system to uncertainty in the servo-valve characteristics and noise. The custom built amplifier used in this application was unable to suppress the noise in the system itself; therefore, the sensitivity of the system must be reduced to decrease the effects of noise. Furthermore, with a small input voltage range, there are resolution issues regarding the digital to analog conversion. Allowing flow through the needle valve reduces the system gain (i.e., the input voltage range is increased). Decreasing the gain of the system reduces the effects of the uncertainty, noise, and resolution issues. The flow through the needle valve will, however, increase the steady state (SS) error of the system and waste flow. All but one of the controllers designed in Section 4 have an integrator, which will eliminate the SS error of the CL system.

The needle valve is adjusted until an input of ± 2 V results in a max/min output force of ± 4800 lbf [± 21,351 N] (the noise from the input voltage reading is approximately 0.3 % at this input range). When leakage across the actuator is allowed, the pressure difference between side *A* and *B* of the piston is reduced. Thus, the max/min output force with leakage (± 4800 lbf) is less than the max/min output force without leakage (± 5200 lbf).

3 Experimental Model

An OL linear model of the hydraulic system at a given operating point can be found through experimental process given here.

- Choose an appropriate input voltage signal.
- Run experiment and record input voltage data to the servo-valve amplifier and output force data from the load cell.
- Analyze the input-output data using a fast Fourier transformation (FFT) to find a Bode magnitude and phase plot of the system.
- Once data is collected over a range of frequencies, a TF best representing the OL response of the system is found.

A chirp signal with amplitude of 0.5 V and a frequency range from 0 to 150 Hz is sent to the servo-valve amplifier for a period of 200 seconds. Varying the offset of the chirp signal allows the valve to be tested at different operating points to find a linear model that best represents the system over a range of inputs. Three separate chirp signals with offsets at 0.25, 0 and - 0.25 V are used for testing. Once the experiments are complete, the input and output data are analyzed using a FFT to obtain the Bode magnitude and phase plots shown in Fig. 3 and 4, respectively (refer to "Chirp Data"). The results for the chirp signals with input offsets at 0.25, 0 and - 0.25 V are represented by trial (a), (b) and (c), respectively. The response of the system is negligible at frequencies > 100 Hz; therefore, only data ≤ 100 Hz is considered. As the frequency increases, the range of the experimental data increases (i.e., there is a larger uncertainty associated with data at higher frequencies). Averaging the magnitude and phase data results in a set of closely packed data points representing the mean of the experimental results (see "Filtered Chirp Data" in Fig. 3 and 4).

The OL frequency domain performance can also be found using standard sine waves. A sine wave with a frequency ≤ 100 Hz and magnitude of 0.5 V is first sent to the servo-valve amplifier. The magnitude and phase lag of the system can then be found by directly comparing the input and output signals. The drawback of this test is that several experiments are required to obtain the OL response over the desired frequency range. In contrast, the sine test is useful in verifying the data acquisition process used with the chirp signals. The magnitude and phase results for the sine tests are shown as "*" in Fig. 3 and 4, respectively.

A linear TF that best matches the system characteristics can now be found. Magnitude and phase values at frequencies of 0.1, 1, 5, 10, 25, 50, 75 and 100 Hz are selected from the filtered chirp data and inputted into the Matlab® command *fitsys*, which uses least squares fit to find a TF that best represents the experimental data. The command *fitsys* fits frequency response data with a TF of order *n* using frequency dependent weights, which are used as weighting for the least squares fit. Weights ranging from 0 to 1 were chosen at each of the frequencies given above. These weights were chosen via trial-and-error in finding a TF (refer to Eq. 2 and 3 below) that best fits the experimental data.

It is desired to have a single TF that approximates the frequency domain performance of the system at each operating point. Trial (b) corresponds to the input signal with an offset of 0 V, which is bounded by trials (a) and (c) with offsets of 0.25 and -0.25 V, respectively. Given the nonlinearities that exist in the servo system, models designed at two separate offsets will tend to differ more as the distance between the offsets increase. Therefore, a TF designed with data from trail (b), as opposed to trial (b) or (c), is expected to more closely model the response of the system at all three offsets.

Transfer function models: A 3rd-order, G_3, and 4th-order, G_4, model of the servo system found using data from trial (b) are given as

$$G_3 = \left(\frac{1.705 \times 10^4 (s - 445)}{(s^2 + 365s + 1.705 \times 10^4)(s + 445)} \right) DC \qquad (2)$$

$$G_4 = \left(\frac{(3.283s^2 + 1352s + 2.624 \times 10^6)(s - 2000)}{(s^3 + 363s^2 + 6.894 \times 10^4 s + 2.624 \times 10^6)(s + 2000)} \right) DC \qquad (3)$$

where *DC* is the DC-gain of the system. Both models closely match the experimental phase data for each trial

over the full range of frequencies (see Fig. 4). Only G_4 matches the experimental magnitude data over all frequencies (see Fig. 3). At approximately 20 Hz G_3 begins to diverge away from the experimental magnitude results, which suggests that the system behaves as a higher order model (i.e., $n > 3$) at higher frequencies. Nevertheless, G_3 is not discarded given that it is a good representation of the system at lower frequencies.

The linear models given in Eq. 2 and 3 contain a RHP zero associated with a 1st-order time delay approximation given as

$$e^{-\theta s} \approx \frac{s - 2/\theta}{s + 2/\theta} \tag{4}$$

where θ is the time delay in seconds (Skogestad and Postlethwaite, 2005). The time delays for G_3 and G_4 are 4.5 and 1 ms, respectively, chosen by trial and error to achieve the best fit to experimental data. The difference in time delay between G_3 and G_4 is due mainly to unmodeled dynamics associated with the 3rd-order model, which influence the time delay approximation. A system with a time delay (i.e., RHP zero) has CL control performance limitations (bandwidth limitations) discussed in Section 4.

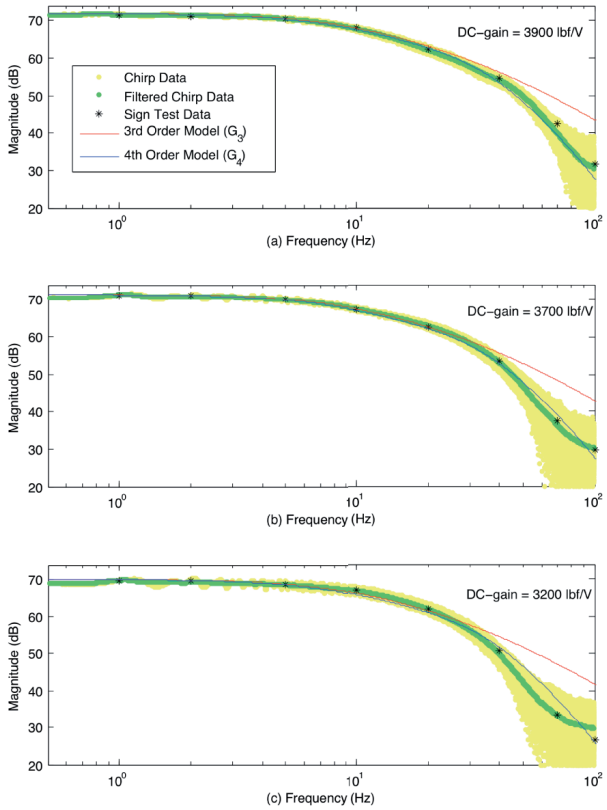

Fig. 3: *Magnitude of the experimental and analytical results*

Steady State Gain: The DC-gain of the system corresponds to the change in output force given a change in input voltage. There are several ways in finding this input-output relationship. The most straightforward procedure is to give the system a constant input voltage and record the corresponding output force. This procedure must be repeated over a range of input voltages. Depending on the initial voltage of the system, the output force at a given input voltage is found to vary. This inconsistency in the output is referred to as hysteresis. The main cause of hysteresis in the case of a servo-valve is static friction or "stiction" between the moving parts of the valve (Manring, 2005). One way to reduce stiction is to keep the valve in constant movement by superimposing a dither signal (i.e., a sine wave) onto the input signal. The magnitude and frequency of the sine wave is chosen to keep the stiction within the valve at a min without influencing the output force signal.

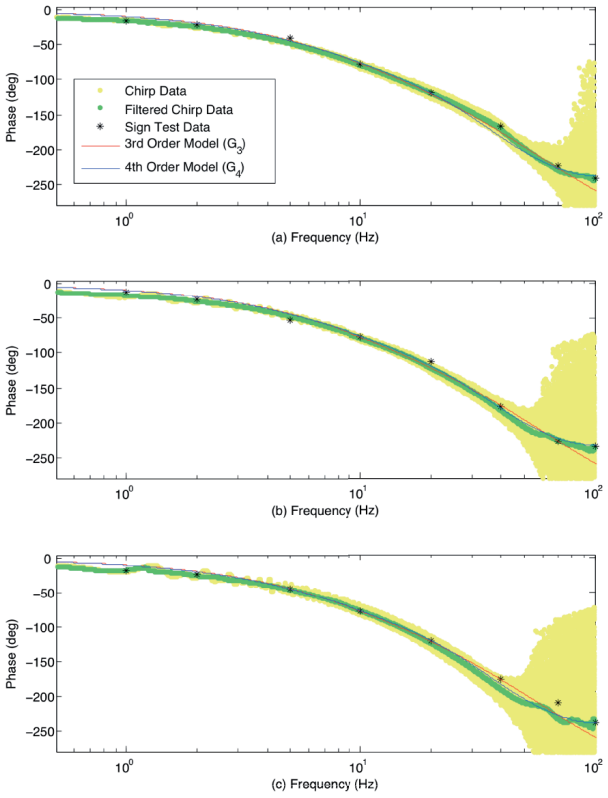

Fig. 4: *Phase of the experimental and analytical results*

Another testing procedure for finding an input-output relationship is to give the system a "slow" moving triangular wave (i.e., the slope of voltage/time is small) over a given range of input voltages. The "slow" triangular wave defines the static relationship between input voltage and output force for increasing and decreasing voltages. Again, hysteresis results from the inconsistencies in the system response as the input voltage is increased (positive slope) and decreased (negative slope). Therefore, a dither signal is also applied to the triangular input wave. A dither signal of amplitude 0.4 V and frequency 175 Hz is found to best reduce the hysteresis for both the static and triangular tests without affecting the output force signal.

The input voltage vs. output force plot for the static and triangular tests are shown in Fig. 5. The static input-output test is performed over an input range from -1 to 1 V at increments of 0.1 V. For each test voltage, the system is stepped from an initial voltage of ± 2 V, which denotes the outer operational bounds of the system. Even with the dither signal superimposed onto the input voltage, the hysteresis of the system is still evident (especially at voltages < -0.5 V). The triangular input-output test is performed over an input range from -2 to 2 V to show the behavior of the DC-gain as the

input voltage reaches the outer bounds of the system. Here, the hysteresis magnitude is significantly larger than from the static test. There are also sharp jumps in the force data at input voltages around 1.2 V. These may be a result of the valve sticking and then releasing as the input voltage continues to change.

Polynomials, P_s and P_t, are fit through the data points in Fig. 5 to find an average force vs. voltage relationship for the static and triangular tests, respectively. The derivatives of P_s and P_t represent the DC-gain curves of the system for each test (see DC-gain vs. Input Voltage plot in Fig. 5). The plots of dP_s and dP_t differ slightly in shape and magnitude, yet their general trends are similar (i.e., they both increase and decrease over similar voltage ranges). The DC-gain of the system does not remain constant over the entire range of input voltages. As shown in Fig. 5, the DC-gain is at a max near 0.6 V and decreases as the voltage is increased or decreased. This decline in the DC-gain is mainly due to the leakage across the actuator. As the input voltage approaches ± 2 V, more fluid is leaked past the needle valve. This increased flow reduces the pressure drop across the valve, resulting in a decreased flow gain. Therefore, the DC-gain of the system will decrease as the input voltage approaches ± 2 V. At voltages beyond ± 2 V, the system response is insignificant.

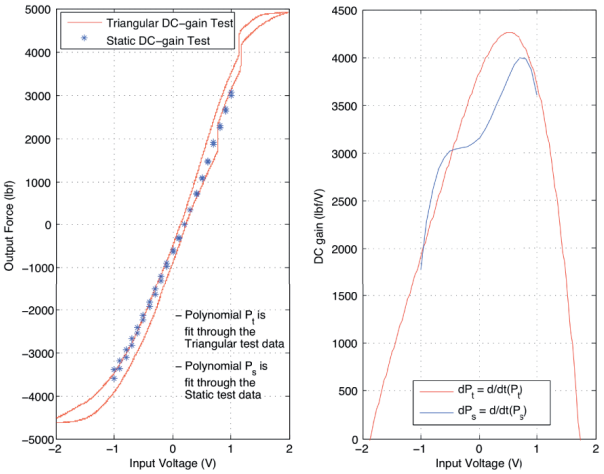

Fig. 5: *Output force (left) and DC-gain (right) as a function of input voltage*

Table 1: Average DC-gain values in lbf/V [N/V]

	Trial (a)	**Trial (b)**	**Trial (c)**
System	3900 [17,348]	3700 [16,458]	3200 [14,234]
Static Test (dP_s)	3700 [16,458]	3300 [14,680]	3090 [13,745]
Triangular Test (dP_t)	3960 [17,615]	3720 [16,547]	3360 [14,946]

The average DC-gain values of the system for trials (a-c) are equivalent to the low frequency response magnitudes given in Fig. 3. The average DC-gain can also be found through the use of the DC-gain polynomials, dP_s and dP_t. A sine wave with the same magnitude and offset as the chirp signals in trials (a-c) is used to evaluate each polynomial. The mean DC-gain output from each polynomial is considered the average DC-gain. Table 1 shows the average DC-gain values of the system and polynomials. Polynomial dP_t reasonably estimates the actual DC-gain of the system, while dP_s underestimates the system gains. The uncertainty in the DC-gain is taken into consideration in determining the robust stability/performance in Section 6.

4 Control Design

Bandwidth Limitation: The OL models found in Section 3 contain a RHP zero on the real axis due to the 1st-order time delay approximation. Therefore, a bandwidth limitation is placed on the control system. For a system with a real RHP zero, z, the achievable bandwidth frequency, ω_B^*, is given as

$$\omega_B^* < z\frac{1-1/M}{1-A} \tag{5}$$

where M and A are the respective high and low frequency performance requirements as defined by the performance weight TF (Eq. 21) discussed in Section 6 (Skogestad and Postlethwaite, 2005). In short, M and A represent the magnitude of a TF at high and low frequencies, respectively. If the error of the system exceeds the magnitude of this TF at any frequency, the system does not meet the performance requirements.

Since model G_4 better represents the OL response of the servo system (see Fig. 3 and 4), the time delay corresponding to RHP zero of G_4 (318 Hz) is a more accurate approximation. Setting M = 3 (allow 300% error at high frequencies) and A = 0.1 (allow 10% error at low frequencies), the max achievable bandwidth is found to be 235 Hz. To achieve the performance requirements given above, a CL bandwidth frequency, ω_B, less than 235 Hz is required. A linear system with ω_B > 235 Hz will have inadequate performance, and as the bandwidth approaches 318 Hz the linear system will become unstable. This theoretic bandwidth limitation assumes an entirely linear system. The effects of the nonlinear DC-gain and input saturation on the achievable bandwidth are discussed in Section 7.

Controller Overview/Selection: Four controllers are considered in improving the performance of the CL control system. The controllers include a Proportional (*P*) controller, Proportional-Integral-Derivative (*PID*) controller and two separate H_∞ controllers. The *PID* controller is expressed in the form

$$K_{PID} = K_P\left(1+\frac{K_I}{s}+K_D s\right) \tag{6}$$

where K_P, K_I and K_D are the proportional, integral and derivative controller gains, respectively. Gains of K_P = 2.7 x 10^{-4}, K_I = 40 and K_D = 2.5e-2 are used in Section 5 for analyzing the time domain performance of the models and system.

To increase the robustness of a control system, H_∞ loop-shaping design is performed to find a controller that optimally improves robustness of a shaped plant. A shaped plant is a linear model multiplied by some type of controller. The controller within the shaped plant

"determines such overall characteristics as response speed, damping characteristics and steady-state error" of the CL system, while the H_∞ controller is used to compensate for uncertainties (Lu and Lin 1993). Through the loop shaping procedure, the H_∞ controller, K_H, is defined as

$$K_H = \left[\frac{A + BF + \gamma^2 (L^T)^{-1} Z C^T (C + DF)}{B^T X} \middle| \frac{\gamma^2 (L^T)^{-1} Z C^T}{-D^T} \right] \quad (7)$$

$$F = -S^{-1}(D^T C + B^T X) \quad (8)$$

$$L = (1 - \gamma^2) I + XZ \quad (9)$$

where A, B, C, D is the state-space representation of the shaped plant, Z and X are unique positive definite solutions to the Riccati equations

$$(A - BS^{-1}D^T C)Z + Z(A - BS^{-1}D^T C)^T - ZC^T R^{-1} CZ + BS^{-1}B^T = 0 \quad (10)$$

$$(A - BS^{-1}D^T C)^T X + X(A - BS^{-1}D^T C) - XB^T S^{-1} B^T X + C^T R^{-1} C = 0 \quad (11)$$

$$\gamma > \gamma_{\min} = (1 + \rho_s(XZ))^{1/2} \quad (12)$$

where ρ_s is the spectral radius of the shaped plant. The Matlab® M-file *coprimeunc* given by Skogestad and Postlethwaite (2005) uses the robust control toolbox along with Eq. 7 to 12 in obtaining an optimal H_∞ controller for a given shaped plant. Controller K_{PID} and the linear models G_3 and G_4 are used in finding two separate H_∞ controllers (i.e., $K_{PID}G_3$ and $K_{PID}G_4$ are the shaped plants from which the H_∞ controllers are designed). The controllers are given as

$$K_{H3} = \frac{229.7s^2 + 1.334\times10^5 s + 6.305\times10^6}{s^3 + 972.4s^2 + 3.579\times10^5 s + 1.49\times10^7} \quad (13)$$

$$K_{H4} = \frac{231.9s^2 + 7.484\times10^4 s + 9.687\times10^6}{s^3 + 601.7s^2 + 1.993\times10^5 s + 2.068\times10^7} \quad (14)$$

where K_{H3} is the H_∞ controller found from $K_{PID}G_3$ and K_{H4} is the H_∞ controller found from $K_{PID}G_4$.

5 Closed-Loop Performance

The time domain performance is found by analyzing the response of each CL control systems to a step input of magnitude 2000 lbf [8,896 N]. The desired force signal steps from -1000 lbf [-4448 N] to 1000 lbf [4448 N] and then back down to -1000 lbf. The result is a step response for both an increasing and decreasing force. The step response of the system and models with *P*, *PID* and H_∞ control are given in Fig. 7 to 9, respectively. As stated in Section 3, the DC-gain does not remain constant for different input voltages. However, a DC-gain of 3100 lbf [13,790 N] is found to be a reasonable approximation for the step input given here. The variations between the time domain response of the system and models (see Fig. 7 to 9) are mainly due to this constant DC-gain assumption. In reality, the DC-gain is continually changing as the input voltage changes, which will change the response of the system (this is a non-linear trait of the system).

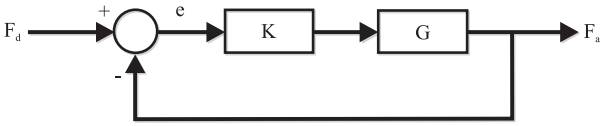

Fig. 6: *CL step responses with P control from -1000 to 1000 lbf (top) and 1000 to -1000 lbf (bottom)*

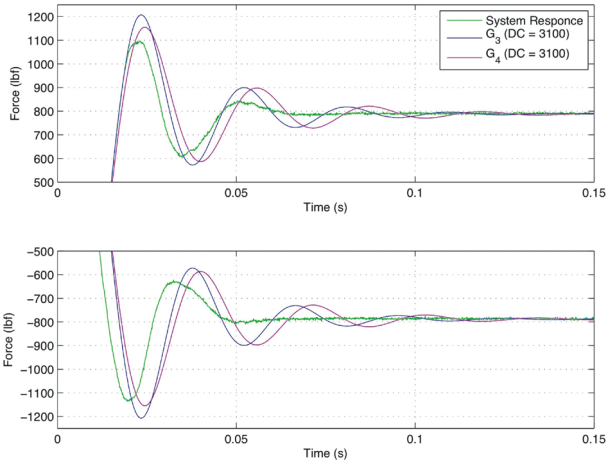

Fig. 7: *CL step response PID control from -1000 to 1000 lbf (top) and 1000 to -1000 lbf (bottom)*

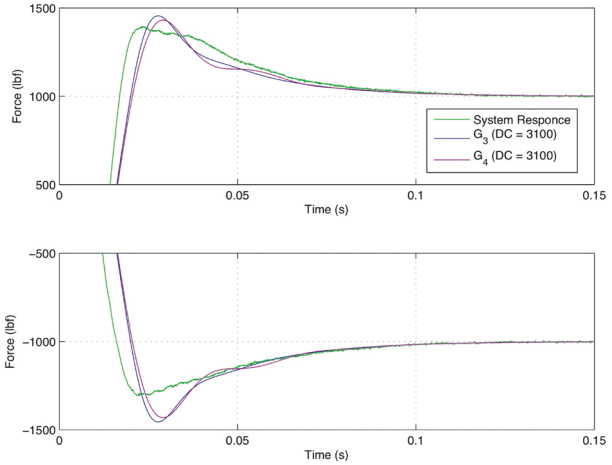

Fig. 8: *CL step response with H_∞ control from -1000 to 1000 lbf (top) and 1000 to -1000 lbf (bottom)*

The time domain performance characteristics for all step response data are given in Table 2. The system has a small rise time, settling time and overshoot with controller K_P; however, the SS error associated with *P* control is a major drawback. Using K_{PID} reduces the rise time and eliminates the SS error, but the settling time and overshoot are increased significantly. This large overshoot is due to a large K_I gain, which was chosen to decrease the rise time of the *PID* control system as much as possible. The *PID* controller is part of the shaped plants used in designing the H_∞ controllers. Therefore, decreasing the rise time of the shaped plants will ultimately decrease the rise time of the H_∞ control systems. As shown in Table 2, the H_∞ control systems also eliminate SS error and have much smaller overshoots than the other control systems (the H_∞ loop-shaping design discussed in Section 4 eliminates the large overshoot caused by K_{PID}). The H_∞ control systems do, however, have the largest rise and settling times.

Table 2: Time domain performance for system and models

		Rise Time (ms)	Settling Time (ms)	Over-shoot (%)	SS error (%)
P Control (K_P)	System	17.1	56.4	6.1	10.6
	G_3	16.6	71.3	9.8	10.6
	G_4	16.5	89.0	13.1	10.6
PID Control (K_{PID})	System	15.8	89.1	19.7	0
	G_3	18.4	80.8	22.8	0
	G_4	18.7	82.1	21.6	0
H_∞ Control (K_{H3} and K_{H4})	System w/ K_{H3}	18.6	96.1	1.9	0
	System w/ K_{H4}	17.8	91.7	2.2	0
	G_3 w/ K_{H3}	26.6	44.8	0	0
	G_4 w/ K_{H4}	24.4	34.2	0.8	0

Frequency Domain Performance: The frequency domain performance is characterized via the CL bandwidth frequency, ω_B, of the system. Large bandwidths usually correspond to a faster response (i.e., faster rise times and settling times) since high-frequency input signals are more easily passed on to the outputs of the system. Consequently, systems with large bandwidths are also more susceptible to noise or uncertainties in the system. Small bandwidths correspond to a slower response with an increased ability to adjust to uncertainty (i.e., an increased robustness).

The control systems found in Section 4 are designed using the linear TF's found from the OL chirp signal data in Section 3, more precisely trial (b), which corresponds to an input chirp signal of magnitude 0.5 V and offset of 0 V. At low frequencies, the OL chirp signal results in a force output magnitude of approximately 1850 lbf [8,230 N] at an offset of -400 lbf [-1,780 N]. To have an accurate comparison of the OL and CL systems, the desired force signal (chirp signal) for each CL control system will have a magnitude and offset equal to the low frequency OL output (i.e., the desired force signal is a chirp signal with magnitude 1850 lbf and offset -400 lbf). Bode magnitude and phase plots for each CL control system can be found through the same process outlined in Section 3 for the OL system. For easy comparison to the CL control cases, the OL Bode magnitude response is normalized. The full input range of the system (-2 to 2 V) is used in analyzing the CL frequency domain performance to give an overall increase in system performance. The magnitude and phase lag of the normalized OL and CL control cases are given in Fig. 10 and 11, respectively. The resulting bandwidth frequencies of the system and models are given in Table 3.

Table 3: Bandwidth frequencies for the OL and CL frequency response and corresponding saturation frequencies

		OL	CL w/K_P	CL w/K_{PID}	CL w/K_{H3}	CL w/K_{H4}
Bandwidth Freq. (Hz)	System	6.9	46.4	40.5	28.2	38.1
	G_3	8.5	46.8	41.1	26.6	-
	G_4	7.8	38.1	34.4	-	25.9
Saturation Freq. (Hz)	System	-	32.5	15.1	>50	33.3
	G_3	-	21.3	21.2	>50	-
	G_4	-	20.8	21.3	-	34.1

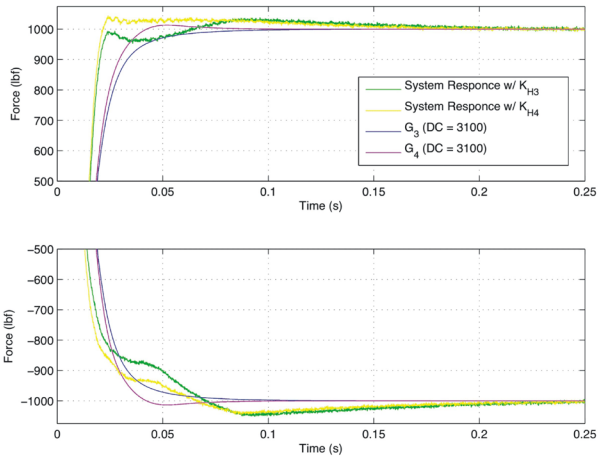

Fig. 9: *Magnitude plot of the normalized OL and CL responses (from top to bottom: P, PID and H_∞ control)*

As shown in Fig. 9, the CL magnitude response of the system and model G_4 have very similar slopes at higher frequencies, which is most evident with *P* and *PID* control. The CL magnitude response of model G_3 has a smaller slope at higher frequencies due to the inaccuracy of the 3rd-order model in the OL magnitude response (see Fig. 3). The phase plots of the system and models (shown in Fig. 10) all have similar slopes at higher frequencies due to the OL phase accuracy of both models (see Fig. 4). The main differences between the frequency domain response of the system and models are the resonant frequencies for the magnitude (i.e., the frequency at which the system oscillates at a max amplitude) and the drop-off frequencies for the phase (i.e., the frequency at which the phase begins to decrease at an accelerated rate). Both the resonance and drop-off frequencies are smaller for the models than they are for the system. These differences can once again be attributed to the assumption of a constant DC-gain. In fact, the gain of the system is continually changing as the frequency and magnitude of the input voltage to the servo-valve amplifier changes (the gain changes with magnitude due to the gain nonlinearities).

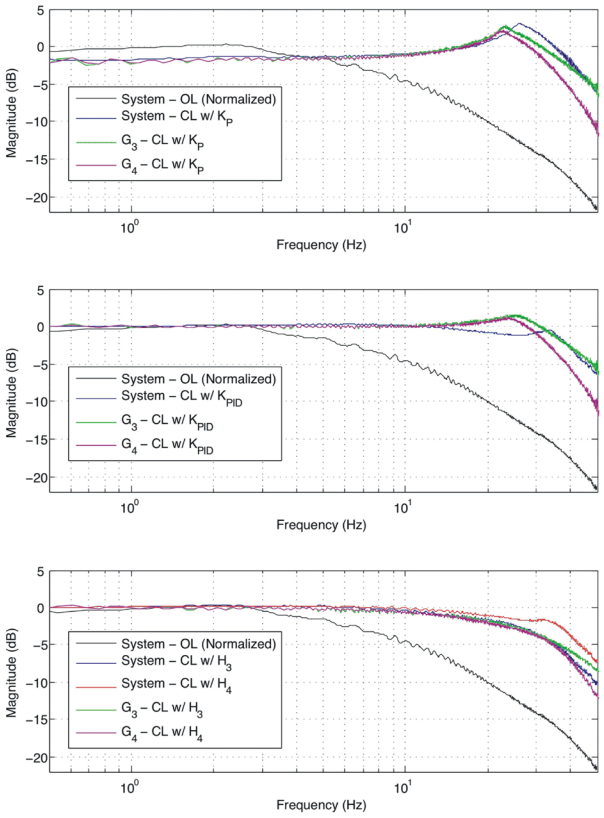

Fig. 10: *Phase plot of the normalized OL and CL responses (from top to bottom: P, PID and H_∞ control)*

As shown in Table 3, the servo system has bandwidths from largest to smallest with controllers K_P, K_{PID}, K_{H4} and K_{H4}, respectively. Therefore, controller K_P and K_{PID} provide the system with a faster response (better performance), which corresponds to faster rise times in the time domain. In contrast, controllers K_{H3} and K_{H4} increase the stability of the system (better robustness), which corresponds to small overshoots in the time domain. The saturation frequency of the system and models (i.e., the frequency at which the input voltage reaches ± 2 V) is also noted in Table 3 for each CL control system. The only controller that does not cause the system to saturate is K_{H3}, which is also the controller that results in the smallest CL bandwidth. Control systems with small bandwidths do not have the tendency to amplify the error signal as much as higher bandwidth systems (i.e., they are less likely to saturate as the error signal increases in magnitude). Decreasing the magnitude of the CL chirp signal (desired force signal) will decrease the amount of saturation the system experiences. However, for sake of comparing the OL and CL responses, reducing the CL chirp magnitude requires an OL response with a smaller output force magnitude (i.e., the OL chirp input voltage magnitude must be reduced).

6 Stability and Performance Robustness

Uncertainties: To characterize the stability and performance of each control system, the uncertainties in the system must first be defined. There are two main uncertainties that exist in the servo system: a dynamic (frequency-dependent) uncertainty in the experimental chirp data and a parametric (real) uncertainty in the DC-gain. The dynamic uncertainty is represented as a multiplicative uncertainty (MU) of the form

$$G_{p,d} = G_n(1 + w_I\Delta_I),\ |\Delta_I(j\omega)| \le 1 \quad \forall\omega \tag{15}$$

where $G_{p,d}$ is the dynamically perturbed plant (i.e., the experimental chirp data), G_n is the nominal plant (i.e., the TF model of the system), w_I is a TF used in modelling the dynamic uncertainty, Δ_I is any stable TF such that $\|\Delta_I\|_\infty \le 1$ and ω is the frequency. The dynamic uncertainty TF, w_I, is found from the relationships

$$l_I(\omega) = \max_{G\in\Pi}\left|\frac{G_{p,d}(j\omega) - G_n(j\omega)}{G_n(j\omega)}\right| \tag{16}$$
$$|w_I(j\omega)| \ge l_I(\omega), \forall\omega$$

where l_I is the max MU from the chirp data. Since the 4th order model G_4 matches the experimental OL chirp data over the entire experimental frequency range, it will represent the nominal plant. The MU from each chirp signal (trial (a-c)) is shown in Fig. 11. The data in Fig. 11 represents a relatively small range of input voltage offsets (-0.25 to 0.25 V). This was done to keep the input vs. output relationship shown in see Fig. 5 as close to linear as possible. Therefore, Fig. 5 represents a limited range of possible MU's (i.e., the MU's would be larger if the entire voltage range was considered).

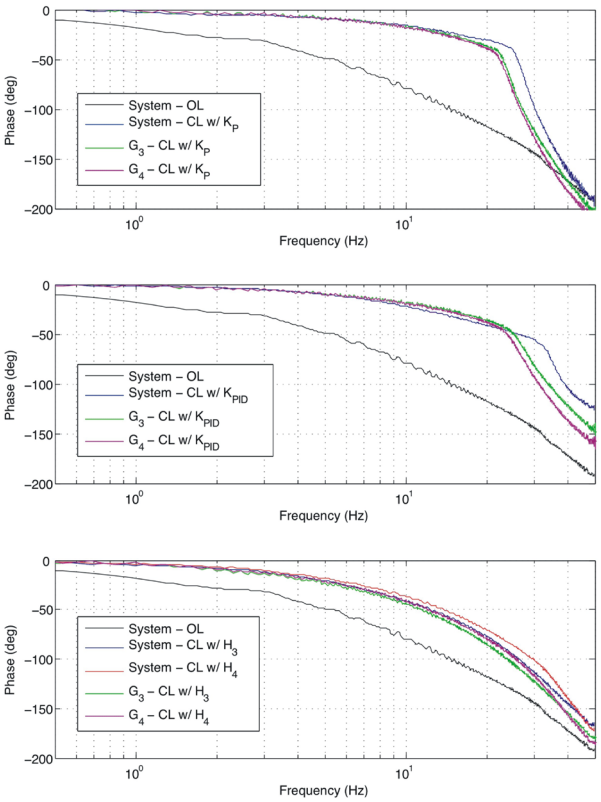

Fig. 11: *Dynamic MU for trials (a-c) and uncertainty TF*

As defined in Eq. 16, the magnitude of w_I must be greater than or equal to l_I over all frequencies (i.e., w_I represents the least upper bound of dynamic uncertainty over the entire frequency range). The *fitmag* command in Matlab®, which fits a stable TF with min phase to a set of magnitude data points, is used in finding a 3rd-order TF, w_I, that bounds all dynamic uncer-

tainties associated with the experimental chirp data (see Fig. 11). The TF form of w_I is defined as

$$w_I = \frac{8.892s^3 + 7825s^2 + 6.49e6s + 1.304e9}{s^3 + 5254s^2 + 1.553e6s + 2.231e9} \quad (17)$$

The parametric gain uncertainty in MU form is written as

$$G_{p,p} = G_n(1 + r_k\Delta), |\Delta| \le 1 \quad (18)$$

where $G_{p,p}$ is the parametrically perturbed plant, Δ is a real scalar and r_k is the relative magnitude of the gain uncertainty defined by

$$r_k = \frac{(k_{max} - k_{min})}{(k_{max} + k_{min})} \quad (19)$$

where k_{max} and k_{min} are the max and min gain values, respectively. As shown in Section 3, the input voltage range affects the min and max DC-gain of the system. Three separate input voltage ranges (± 2, ± 1 and ± 0.5 V) are used to show how changing the input range influences the robust stability/performance of the control systems. Referring to polynomial dP_t in Fig. 5, input ranges of ± 2, ± 1 and ± 0.5 V result in min/max gains of 0/4250 [0/18,905], 1930/4250 [8,585/18,905] and 3420/4135 lbf/V [15,213/18,393 N/V], respectively. Therefore, the relative gain uncertainty magnitude, r_k, for the respective input ranges is 1, 0.379 and 0.095. Reducing the input range reduces the amount of parametric uncertainty; however, doing so will limit the performance of the system.

Performance Weight: A block diagram of the servo system with both dynamic and parametric uncertainties is shown in Fig. 12 (G_p is the plant perturbed by both dynamic and parametric uncertainties). To analyze the performance of the system, a performance weight TF, w_P, is also needed. The performance weight is written as

$$w_P = \frac{s/M + \omega_{BR}}{s + \omega_{BR}A} \quad (20)$$

where M is the allowable error at high frequencies, A is the allowable error at low frequencies and ω_{BR} is the approximate bandwidth requirement. The inverse of w_P represents the upper bound of the sensitivity, $|S|$. The sensitivity function, S, is the TF between the reference input and error in Fig. 12 given as

$$S = \frac{1}{1 + G_pK} \quad (21)$$

In order for the system to meet the performance requirements defined by w_P, the H_∞ norm of the weighted sensitivity function, w_PS, must be less than 1. Alternatively, $|S|$ must be less than $1/|w_P(j\omega)|$ (Skogestad and Postlethwaite, 2005). Smaller values of ω_{BR} will increase the allowable error at lower frequencies, and vice versa. A CL system that is capable of maintaining performance at the largest possible value of ω_{BR} (i.e., a system able to accurately track higher frequency input signals) is desired. In regards to the servo system, locating w_P on the error signal (see block diagram in Fig. 12) allows the performance of the system to be gauged by the difference between desired force input and actual force output. The error signal is fed through the w_P block and a fictitious uncertainty block, Δ_P, before it is sent back to the input of the system (see Fig. 12). If the magnitude of the error signal is larger than $1/|w_P(j\omega)|$ at a given ω, the servo system does not maintain the specified performance requirements.

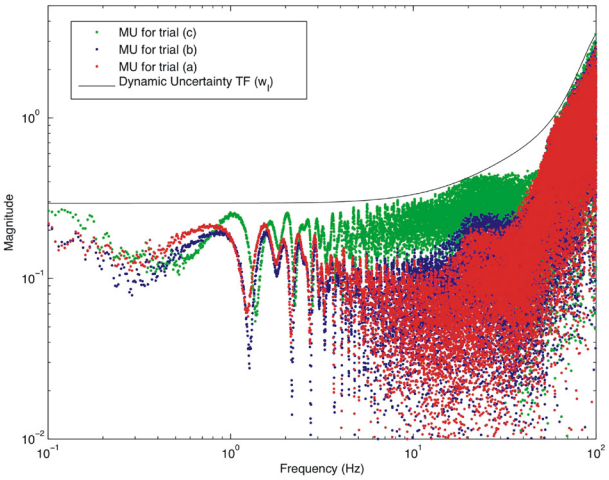

Fig. 12: *CL system with MU's and performance on the error*

The Block diagram in Fig. 12 can now be analyzed to obtain the generalized plant model P. Plant P has 4 inputs (u_Δ, $u_{\Delta I}$, $u_{\Delta P}$ and v) as 4 outputs (y_Δ, $y_{\Delta I}$, $y_{\Delta P}$ and u). The matrix form of this equation is given below.

$$\begin{Bmatrix} u_\Delta \\ u_{\Delta I} \\ u_{\Delta P} \\ v \end{Bmatrix} = \begin{bmatrix} 0 & 0 & 0 & r_k \\ w_I & 0 & 0 & w_I \\ -w_PG_n & -w_PG_n & w_P & -w_PG_n \\ -G_n & -G_n & 1 & -G_n \end{bmatrix} \begin{Bmatrix} y_\Delta \\ y_{\Delta I} \\ y_{\Delta P} \\ u \end{Bmatrix} \quad (22)$$

The P-matrix can be partitioned into the following elements.

$$P_{11} = \begin{bmatrix} 0 & 0 & 0 \\ w_I & 0 & 0 \\ -w_PG_n & -w_PG_n & w_P \end{bmatrix} \quad P_{12} = \begin{bmatrix} r_k \\ w_I \\ -w_PG_n \end{bmatrix} \quad (23)$$

$$P_{21} = \begin{bmatrix} -G_n & -G_n & 1 \end{bmatrix} \quad P_{22} = \begin{bmatrix} -G_n \end{bmatrix} \quad (24)$$

The lower linear fractional transformation is now used in obtaining the N-matrix.

$$N = P_{11} + P_{12}K(I - P_{22}K)^{-1}P_{21} \quad (25)$$

Similar to the P-matrix, the N-matrix is partitioned into 4 elements (N_{11}, N_{12}, N_{21} and N_{22}). Element N_{11} contains information regarding the uncertainties of the system (i.e., r_k and w_I), while element N_{22} contains the performance requirements of the system (i.e., w_P). The off diagonal elements N_{12} and N_{21} may contain uncertainty and/or performance information.

Stability: The stability of the servo system is tested for input voltage ranges of ± 2 V (r_k = 1), ± 1 V (r_k = 0.379) and ± 0.5 V (r_k = 0.095). The N-matrix for each control system has eigenvalues in the LHP when r_k equals 0.095, 0.379 and 1. Therefore, each controller provides NS to the CL system for input voltage ranges up to ± 2 V. The RS of the control systems at each value of r_k is determined through the structured singular values of N_{11} over a frequency range from 0 to 100 Hz (see Fig. 13). All controllers are found to provide

RS (i.e., $\mu_{\bar{\Delta}}(N_{11}(\omega)) < 1 \,\forall\, \omega$) when r_k = 0.095 and r_k = 0.379. However, when r_k = 1, controllers K_P and K_{PID} are unable to maintain stability for all perturbed plants (i.e., $\mu_{\bar{\Delta}}(N_{11}(\omega)) > 1$ for certain ω values). Small values of $\mu_{\bar{\Delta}}(N_{11}(\omega))$ correlate to system with better RS (i.e., a larger "additional" perturbation is needed to cause $\mu_{\bar{\Delta}}(N_{11}(\omega)) = 1$).

As shown in Fig. 13, controller K_P has the best RS at small ω values. Yet, the H_∞ controllers, K_{H3} and K_{H3}, have better RS for any ω > 10 Hz, which is a result of the robust characteristics of the H_∞ control. Both K_P and K_{PID} have resonance peaks near 30 Hz that cause the control systems to fail the RS criteria when r_k = 1 (see Fig. 13). These resonance peaks also show up in the CL frequency domain performance plot in Fig. 9. Table 4 gives the NS and RS for each control system.

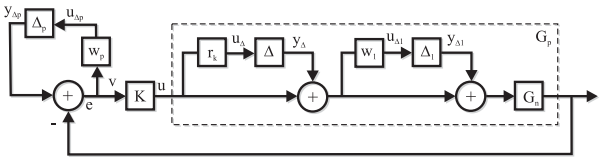

Fig. 13: *Robust stability for r_k = 0.095, 0.379 and 1*

Table 4: Stability and performance of each control system

	Controller	NS	RS	NP	RP
Input ±0.5 V r_k = 0.095	KP	Yes	Yes	Yes (ωBR ≤ 5.2 Hz)	No
	KPID	Yes	Yes	Yes (ωBR ≤18.1 Hz)	No
	KH3	Yes	Yes	Yes (ωBR ≤10.6 Hz)	Yes (ωBR ≤ 6.6 Hz)
	KH4	Yes	Yes	Yes (ωBR ≤11.9 Hz)	Yes (ωBR ≤ 7.4 Hz)
Input ±1 V r_k = 0.379	KP	Yes	Yes	" "	No
	KPID	Yes	Yes	" "	No
	KH3	Yes	Yes	" "	Yes (ωBR ≤ 3.5 Hz)
	K_{H4}	Yes	Yes	" "	Yes (ω_{BR} ≤ 2.5 Hz)
Input ±2 V r_k = 1	K_P	Yes	No	" "	No
	K_{PID}	Yes	No	" "	No
	K_{H3}	Yes	Yes	" "	No
	K_{H4}	Yes	Yes	" "	No

Performance: The performance is also tested for r_k equal to 1, 0.379, and 0.095. The performance of each control system is dependant on the performance weight TF, w_P. Referring to Fig. 12, w_P is placed on the error signal; therefore, the magnitude of the error will determine if the system meets the given performance requirements. The allowable errors are set at 10 % (A = 0.1) for low frequencies and 300 % (M = 3) for high frequencies (the same values of A and M are used in defining the bandwidth limitation in Section 4). The performance of each control system is tested at different values of the ω_{BR} (bandwidth requirement) to find at what bandwidth each system is considered to have NP and RP.

The NP (i.e., $\bar{\sigma}(N_{22}(\omega)) \,\forall\, \omega$) for each control system is illustrated in Fig. 14 for ω_{BR} = 10 Hz. The *PID* controller has better NP for any ω < 30 Hz, while the H_∞ controllers have better NP for any ω > 30 Hz (the NP of the H_∞ controllers increases as ω increases beyond 5 Hz). The *P* controller does not have NP at ω_{BR} = 10 Hz. Once again, K_P and K_{PID} have resonance peaks near 30 Hz that have a negative effect on the NP of the system. Table 4 shows the bandwidths over which each control system maintains NP (since N_{22} does not contain any uncertainty information, each controller has the same NP for the different values of r_k). Controller K_{PID} is able to provide the system with NP over the largest bandwidth (18.1 Hz). Controller K_P has the smallest NP range (5.2 Hz) given the low frequency SS error associated with *P* control. The H_∞ controllers have similar NP bandwidths (10 to 11 Hz).

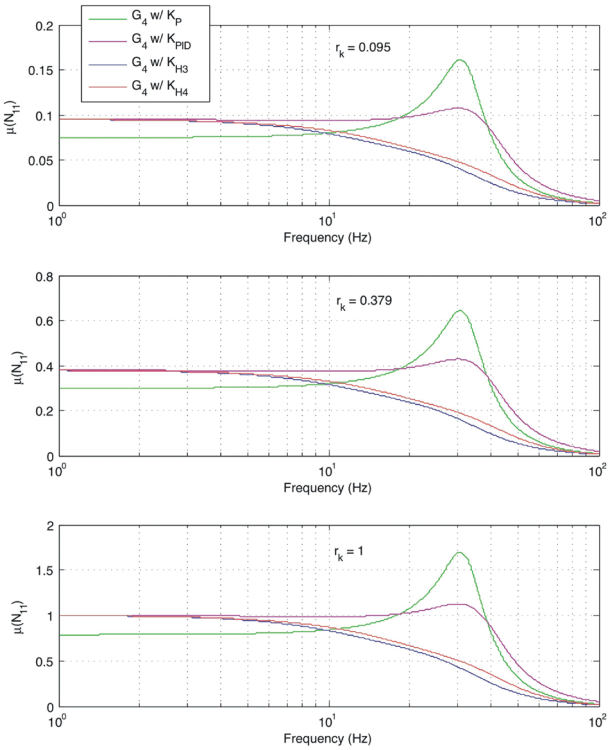

Fig. 14: *Nominal performance with A = 0.1, M = 3 and ω_{BR} = 10 Hz*

A system must have a balance between robustness (good RS) and fast response time (good NP) to qualify for RP. For this reason, if a given CL control system does not have RS or NP, the system will not have RP. Therefore, when r_k = 1, controllers K_P and K_{PID} are automatically disqualified from providing RP. In fact, no control system is able to provide RP when r_k = 1. However, both H_∞ controllers do offer RP when r_k = 0.379 and r_k = 0.095 (see Table 4).

does not have RS or NP, the system will not have RP. Therefore, when r_k = 1, controllers K_P and K_{PID} are automatically disqualified from providing RP. In fact, no control system is able to provide RP when r_k = 1. However, both H_∞ controllers do offer RP when r_k = 0.379 and r_k = 0.095 (see Table 4).

As shown in Table 4, controller K_{PID} has the best NP frequency range, yet K_{PID} is unable to offer RP given that it has RS issues near 30 Hz caused by the resonance peak shown in Fig. 13. Controller K_P does not provide RP given that is has poor NP due to low frequency SS error (see Table 4 and Fig. 14). The H_∞ controllers are able to provide RP given that they have excellent RS and decent NP (see Table 4 and Fig. 14 and 15). Limiting the input voltage range of the servo system, which reduces the significance of the parametric uncertainty by limiting the gain of the system, increases the bandwidth range over which the H_∞ controllers maintain RP. However, by limiting the input voltage, the response of the system will be restricted causing a reduction in the overall performance of the servo system.

7 Conclusion

The OL response of the hydraulic servo system is best represented as the 4th-order linear TF, G_4, containing a 1st-order time delay approximation. The RHP zero associated with the time delay places a bandwidth limitation of 235 Hz on any feedback control system. Therefore, there theoretically exists a controller capable of providing the model with a bandwidth of 225 Hz. The bandwidth limitation analysis is based on a linear TF model; therefore, it does not take into account any non-linear behaviors of the real system such as the deterioration of the DC-gain as the input voltage increases or the saturation of the system. Furthermore, the OL magnitude response of the system is found to be insignificant at any frequency greater than 100 Hz (the same cannot be said for the linear model). The actual bandwidth limitation of the non-linear servo system is, therefore, expected to be at some frequency less than 235 Hz.

The max bandwidth achieved by any control system was 46.4 Hz, which is much smaller than the linear bandwidth limitation. Modifying each controller (i.e. adjusting controller gains) can further increase the CL bandwidth of the system; however, doing so may have an adverse affect on the performance and/or robustness of the system. As the overall gain of a controller is increased, the amount of saturation the system experiences will also increase. When the system saturates, the effectiveness (i.e., the performance) of the control system is diminished. As a result, the non-linear characteristics of the servo system cause the actual bandwidth limitation to be significantly less than what is predicted from the linear model.

Controller K_{H3} provides the lowest CL bandwidth frequency (28.2 Hz) of any control system, meaning it is better able to adjust to uncertainties within the system. This controller also has the best RS over the majority of the frequency ranges. Consequently, it was the only controller not to cause saturation when tracking a chirp signal with magnitude of 1850 lbf [8,230 N], offset of -400 lbf [-1780 N] and frequency range of 50 Hz. The ability of a control system to stay within the active input range of the system (especially at high magnitudes and frequencies) is very desirable. Controller K_{H3} also provides the best RP for the highest input voltage range (± 1 V). Since decreasing the input range has significant affects on CL performance, it is desired to have a control system with the best possible performance at the largest possible input range. Therefore, it is concluded that the best overall control (i.e., the best balance of CL performance and stability) is attained with the H_∞ controller K_{H3}.

Existing dynamic testing units with force ranges similar to the system discussed in this work have bandwidth frequencies from 15 to 55 Hz with 80 % load and 3000 psi [20.68 MPa] supply pressure (MTS Systems, 2009 and Instron, 1998). As discussed above, the H_∞ controllers were able to supply between 28 and 38 Hz at a supply pressure of 1000 psi [6.89 MPa]. Increasing the supply pressure should further increase the performance capability of the system discussed in this work.

It is clear that a higher order control system, such as H_∞ control, is required to obtain satisfactory RP and RS from the hydraulic servo-valve system. The main need for this higher order control is a result of the time delay (RHP zero) that exists in the models of the system.

Acknowledgments

The authors would like to thank C. J. McDonald for his helpful assistance in this work.

Nomenclature

A	Low frequency performance requirement	
A, B, C, D	State-space variable of the plant	
A_o	Cross-sectional area within the needle valve	[m^2]
C_d	Volumetric flow rate through needle valve	[m^3/s]
DC	DC-gain of the servo system	[N/V]
dP_s	Poly. for static DC vs. Input Voltage	
dP_t	Poly. for triangular DC vs. Input Voltage	
G	Plant	
G_3	3rd-order TF of the CL servo response	
G_4	4th-order TF of the CL servo response	
G_n	Nominal plant model	
$G_{p,d}$	Dynamically perturbed plant model	
$G_{p,p}$	Parametrically perturbed plant model	

k_{max}	Max gain value	[N/V]
k_{min}	Min gain value	[N/V]
K	Controller	
K_D	Derivative gain	[sec]
K_H	H_∞ controller	
K_{H3}	H_∞ controller found from $K_{PID}G_3$	
K_{H4}	H_∞ controller found from $K_{PID}G_4$	
K_I	Integral gain	[sec^{-1}]
K_P	P Controller (proportional gain)	[V/N]
K_{PID}	PID Controller	
$K_{PID}G_3$	Shaped plant with 3rd-order model	
$K_{PID}G_4$	Shaped plant with 4th-order model	
L	Any complex matrix	
l_I	Max multiplicative uncertainty	
M	High frequency performance requirment	
n	order of the transfer function model	
N	N-matrix	
P	Generalized plant model (P-matrix)	
P_A	Actuator pressure on the side A	[MPa]
P_B	Actuator pressure on the side B	[MPa]
P_s	Poly. for the static input-output relationship	
P_{su}	Supply pressure from hydraulic power unit	[MPa]
P_t	Poly. of the triangular Input vs Output relation	
Δp	Pressure difference across the needle valve	[MPa]
Q	Volumetric flow rate through needle valve	[m^3/s]
r_k	Relative magnitude of the gain uncertainty	
w_I	Dynamic uncertainty transfer function	
w_P	Performance weight transfer function	
Z, X	Unique definite solutions to Riccati eq.	
Δ	Real scalar	
Δ_I	Stable transfer function such that $\|\Delta_I\| \le 1$	
Δ_P	Fictitious uncertainty block	
ζ	Damping ratio	
θ	Time delay	[sec]
μ	Structured singular value	
ρ	Hydraulic fluid density	[kg/ m^3]
ρ_s	Spectral radius (max singular value)	
$\bar{\sigma}$	Max singular value	
ω	Frequency ranging from 0 to 100 Hz	[Hz]
ω_B	Closed-loop bandwidth frequency	[Hz]
ω_B^*	Acheivable bandwidth	[Hz]
ω_{BR}	Approximate bandwidth requirement	[Hz]
ω_n	Natural frequency	[Hz]

References

Alleyne, A. and **Liu, R.** 1999. On the Limitations of Force Tracking Control for Hydraulic Servosystems, *ASME, Vol. 121*, pp. 184-190.

Cheng, Y. and **De Moor, B. L. R.** 1994. Robust Analysis and Control System Design for a Hydraulic Servo System, *IEEE Proc., Vol. 2, Issue 3*, pp. 183-197.

Chiriboga, J., **Thein, M.-W. L.** and **Misawa, E. A.** 1995. Input-Output Feedback Linearization Control of a Load-Sensing Hydraulic Servo System, *IEEE Proc.*, pp. 910-915.

Djukanovic, M., **Khammash, M.** and **Vitta1, V.** 1997. Structured Singular Value Theory Based Stability Robustness of Power Systems, *IEEE Proc., Vol. 3, Issue 10-12*, pp. 2702-2707.

Doyle, J. C. 1982. Analysis of Feedback Systems with Structured Uncertainty, *IEE Proc., Part D, Vol. 129*, pp. 251-256.

Doyle, J. C., **Wall, J. E.** and **Stein, G.** 1982. Performance and Robustness Analysis for Structured Uncertainty, *IEEE Proc., Vol. 21, Part 1*, pp. 629-636.

Fan, M. K. H. and **Tits, A. L.** 1986. Characterization and Efficient Computation of the Structured Singular Value, *IEEE Proc., Vol. 31, Issue 8*, pp. 734-743.

Instron Corporation. 1998. *8870 Technical Data Book* [Brochure], Norwood, MA: 1998.

Lu, H. C. and **Lin, W. C.** 1993. Robust Controller with Disturbance Rejection for Hydraulic Servo System, *IEEE Proc., Vol. 40, Issue 1*, pp. 157-162.

Manring, N. D. 2005. *Hydraulic Control Systems*, John Wiley & Sons, Hoboken, NJ, 61-64, 156-160, 169-176, 234-252.

MTS Systems Corporation. 2009. *MTS Landmark Servohydraulic Test Systems* [Brochure], Eden Prairie, MN: 2009.

Niksefat, N. and **Sepehri, N.** 1999. Robust Force Controller Design for a Hydraulic Actuator Based on Experimental Input-Output Data. *IEEE Proc., Vol. 5, Issue 2-4*, pp. 3718-3722.

Rito, G. D., **Denti E.** and **Galatolo R.** 2006. Robust Force Control in a Hydraulic Workbench for Flight Actuators, *IEEE Proc., Issue 4-6*, pp. 807-813.

Sideris, A. and **Sanchez Pena, R. S.** 1990. Robustness Margin Calculation with Dynamic and Real Parametric Uncertainty. *IEEE Proc., Vol. 35, Issue 8*, pp. 970-974.

Skogestad, S. and **Postlethwaite, I.** 2005. *Multivariable Feedback Control: Analysis and Design*, John Wiley & Sons Ltd, second edition, 22, 30, 32-34, 38-39, 56, 60-62, 105-110, 127, 186, 306-319, 364-368.

Joseph Kennedy
Received a B.S. and M.S. in Mechanical Engineering from the University of Missouri in 2007 and 2009 respectively. Currently, he is a Ph.D. student at the University of Missouri.

Roger Fales
Received B.S. and M.S. degrees in Mechanical Engineering at Kansas State University in 1996 and 1998 respectively. He was employed at Caterpillar Inc. from 1998 to 2002 as a research engineer. At Iowa State University, he received a Ph.D. in Mechanical Engineering in 2004. In 2004, he joined the Mechanical & Aerospace Engineering Department at the University of Missouri – Columbia. As an assistant professor, he teaches and does research work in the areas of dynamics, systems, automatic control, and fluid power.